Quantum analogue of a Kerr black hole and the Penrose effect in a Bose-Einstein condensate

D. D. Solnyshkov,[1] C. Leblanc,[1] S. V. Koniakhin,[1,2] O. Bleu,[1] and G. Malpuech[1]
[1]*Institut Pascal, University Clermont Auvergne, CNRS, SIGMA Clermont, F-63000 Clermont-Ferrand, France*
[2]*St. Petersburg Academic University–Nanotechnology Research and Education Centre of the Russian Academy of Sciences, 194021 St. Petersburg, Russia*

(Received 15 April 2019; revised manuscript received 13 May 2019; published 24 June 2019)

Analogue physics became very popular in recent decades. It allows simulating inaccessible physical phenomena, such as black holes, in the laboratory. The first success of analogue physics is in fact much older being due to Maxwell, who derived his equations for the electromagnetic field by analogy with fluid dynamics in presence of vortices. Here we propose to use vortices for analogue gravity. We implement an acoustic Kerr black hole with quantized angular momentum in a Bose-Einstein condensate. We show that the condensate's metric is equivalent to the Kerr's one, exhibiting a horizon and an ergosphere. We confirm that this metric is obeyed not only by weak density waves, but also by quantum vortices which behave as massive test particles. We use these topological defects to demonstrate a quantum Penrose effect, extracting the rotation energy of the black hole by quanta of angular momentum. The particle trajectories are well described by the timelike geodesics of the Kerr metric, confirming the potential of analogue quantum gravity.

DOI: 10.1103/PhysRevB.99.214511

I. INTRODUCTION

The field of analogue physics has been growing since the 1980s, when the first proposals were published, linking astrophysical phenomena such as the Hawking emission of black holes [1] or the Kibble mechanism of topological defect formation in the early Universe [2] with desktop systems [3–5]. The long efforts [6,7] were very successful, allowing the recent observation of Hawking emission [8,9] and the observation of the Kibble-Zurek mechanism in various systems [10,11]. Of course, the full spectrum of analogue physics phenomena extends far beyond these two most striking examples [12–15].

Exciton-polariton (polariton) condensates are particularly well suited for analogue physics because this quantum fluid allows a versatile all-optical control of the wave function via external potentials (both real and imaginary), together with the optical means for the measurement of all wave-function components both in real and reciprocal space. Polaritons are light-matter quasiparticles existing in microcavities [16] in the strong-coupling regime. They inherit a small effective mass of photons and strong interparticle interactions from excitons, the former ensuring a large coherence length even in reduced dimensions [17], and the latter providing the means for optical potential engineering [18]. Many proposals for analogue physics based on polaritons have appeared in recent years [19–21], and some of them have already been implemented experimentally [22,23].

A new frontier in analogue physics is the Penrose effect [24], which is the extraction of kinetic energy stored in rotating black holes described by the Kerr metric [25]. The generalized Penrose process might be powering relativistic jets of black holes [26] and influencing their accretion disks, which start to become directly observable [27]. It involves the creation of a pair of positive and negative energy particles, when the particle with negative energy $E < 0$ falls into the black hole, reducing its angular momentum, while the particle with positive energy $E > 0$ escapes to infinity, with the overall process resulting in energy extraction. The region where such a process is possible is called an ergosphere. As a first step, it requires the creation of a Kerr black hole analogue in a fluid [28,29], either classical or quantum. So far, acoustic black holes have been mostly one-dimensional (1D) [9,23,30,31], and only recently 2D black holes with closed horizons have been implemented, which has already allowed to observe [32] the superradiance effect [33]. However, only the propagation of sound waves corresponding to null geodesics has been studied so far. Little attention has been paid in this respect to quantum vortices, which represent an important direction of analogue physics since the 1970s [34]. The story actually dates back to Maxwell, who derived his equations for the electromagnetic field by analogy with fluid dynamics in the presence of vortices [35]—the first success of analogue physics, which now aims to reproduce electrodynamics as an emergent theory in quantum fluids [36], similar to analogue gravity. Described by a relativistic action in a local Minkowski frame [34,37] determined by the speed of sound c, quantum vortices behave as relativistic particles with their dynamics governed by the fluid metric [5,38]. Contrary to high-wave-vector bogolons, which can propagate faster than the speed of sound and thus violate the horizons of the low-wave-vector metric, vortices cannot exceed c [39]. With their mass given by Einstein's relation $E = mc^2$ [34], and their stability ensured by a topological quantum number (winding), vortices therefore appear as excellent candidates to study the timelike geodesics of massive particles in the vicinity of black holes. The dynamics of vortices has been extensively studied experimentally in atomic [40] and polariton condensates [41], but not in the framework of analogue physics.

In this work, we propose to implement a Kerr black hole in a polariton condensate by combining optical excitation with a Gauss-Laguerre beam, providing the angular momentum, and a region of reduced lifetime, creating an inward flow. Similar configurations have already been implemented with polaritons [42,43]. We show that the metric of the condensate in this configuration is equivalent to the Kerr metric of a rotating black hole. We demonstrate that the topological defects of the condensate (quantum vortices) can be used as test particles whose propagation close to the horizon follows the timelike geodesics of the Kerr metric, opening the domain of analogue gravity to the studies of massive particles. We simulate a quantum analogue of the Penrose effect using a vortex-antivortex pair, with an antivortex falling into the black hole and reducing its quantized angular momentum, and a vortex escaping from the black hole to infinity. This represents a step toward self-consistent analogue gravity systems with the metric naturally subject to quantum fluctuations. While we have optimized our proposal for the cavity polariton system, there are no fundamental obstacles for its implementation in other types of quantum fluids, such as atomic condensates [44] or superfluid light [45].

II. THEORETICAL DESCRIPTION

A Bose-Einstein condensate is a quantum fluid that can be described in the mean-field approximation by the Gross-Pitaevskii equation [39]:

$$i\hbar\frac{\partial\psi}{\partial t} = -\frac{\hbar^2}{2m}\Delta\psi + \alpha|\psi|^2\psi + U\psi - \mu\psi, \tag{1}$$

where $\psi(r,t)$ is the condensate wave function, m is the particle mass, α is the interaction constant, U is the external potential (with a possible imaginary part describing particle decay), and μ is the chemical potential. The analogy between the condensate and the general relativity spacetime is based on the fact that the propagation of the weak excitations of a homogeneous stationary condensate can be described by a relativistic wave equation for their phase [46]:

$$\partial_\mu(\sqrt{-g}g^{\mu\nu}\partial_\nu\varphi) = 0 \tag{2}$$

with $g = det(g_{\mu\nu})$, and the metric $g_{\mu\nu}$ totally determined [3] by the background stationary velocity $\mathbf{v} = (\hbar/m)\nabla\arg\psi$ and the local speed of sound $c = \sqrt{\alpha|\psi|^2/m}$:

$$g_{\mu\nu} = \frac{mn}{c}\begin{pmatrix} -(c^2 - \mathbf{v}^2) & \vdots & -\mathbf{v} \\ \cdots & \cdots & \cdots \\ -\mathbf{v} & \vdots & \delta_{ij} \end{pmatrix}. \tag{3}$$

This metric generalizes the local Minkowski frame to the case of spatially varying speed of the flow and speed of sound, and as such is obeyed both by weak density waves with a wavelength $\lambda \gg \xi$ ($\xi = \hbar/\sqrt{2\alpha mn}$ is the healing length) and by vortices.

A. Vortices as massive relativistic particles

The link between the fluid equations with vortices and the Maxwell equations of electrodynamics is deeply rooted in history: Maxwell himself first derived his equations in 1861 assuming that the magnetic field was caused by "molecular vortices" in a fluidlike medium (aether) [35]. A similar derivation was rediscovered by Feynman in 1948 [47]. Dirac suggested in 1951 [48] that the vector potential of the electromagnetic field actually corresponds to the velocity of the aether (and thus the magnetic field is the measure of its vorticity). Since the 1970s [34], the vortices have again moved into the focus of analogue physics with the goal of the formulation of emergent electrodynamics [36].

While the vortex interaction, closely resembling the electromagnetism, is an extremely interesting topic by itself and occupies an important place in the outlook of our work, we are actually interested so far in the regimes where it is negligible with respect to the "free-fall" dynamics in a curved metric. The relativistic action for vortices was first derived in [34] using the Feynman path integral (also called the continual integration) approach [37,49,50] with a separation of variables for a vortex in a stationary condensate:

$$S_0 = -m_V c\sum_i\int ds_i - iq\int\mathbf{A}\cdot\mathbf{j}d^3x - \frac{1}{2c}\int(\nabla\times\mathbf{A})^2 d^3x, \tag{4}$$

where $m_V = E_V/c^2$ is the vortex mass [with $E_V = \pi n\hbar^2\ln(R/\xi)/m$], $q = 2\pi/\sqrt{\alpha}$ is an effective charge (coupling constant), and the summation i is carried out over individual vortices. This result was obtained by mapping the 2 + 1D vortex interaction problem to a 3D magnetostatic problem with an effective vector potential $\mathbf{A}$, where the time-dependent trajectory of each vortex becomes a stationary current $\mathbf{j}$ in 3D space interacting with the other currents via magnetic field defined by $\mathbf{A}$ (using Maxwell's analogy in the opposite sense). The first term of the action is the length of this world line, accounting for the vortex self-energy. This expression is similar to the covariant form of the action for a relativistic electron in an external electromagnetic field defined by a 4-potential A:

$$S = -m_0 c\int ds + \int\frac{e}{c}\frac{dx_\alpha}{ds}A^\alpha ds, \tag{5}$$

where m_0 is the electron's rest mass. Using the Euler-Lagrange equation allows us to write the following equation of motion for a vortex in a reference frame where the homogeneous condensate is at rest:

$$\frac{d^2x^\mu}{ds^2} = \frac{q}{m_V}F^{\mu\beta}\frac{dx^\alpha}{ds}\eta_{\alpha\beta}, \tag{6}$$

where $F_{\mu\nu} = \nabla_\mu A_\nu - \nabla_\nu A_\mu$ is the tensor of the electromagnetic field, $\eta_{\alpha\beta}$ is the Minkowski tensor, and

$$\eta_{\alpha\beta}\frac{dx^\alpha}{ds}\frac{dx^\beta}{ds} = -1, \tag{7}$$

meaning that the evolution is timelike. The Minkowski metric obeyed by the vortex reads

$$ds^2 = c^2dt^2 - dx_i^2. \tag{8}$$

Passing into a moving reference frame with respect to the condensate requires a Galilean transform $x_i' = x_i - v_i t$, which modifies the metric by mixing the time with the spatial

coordinates,

$$ds^2 = c^2dt^2 - \left(dx_i^2 - 2v_i dx_i dt + v_i^2 dt^2\right) = (c^2 - v^2)dt^2 + 2v_i dx_i dt - dx_i^2. \quad (9)$$

Allowing the condensate density (and thus the speed of sound c) and the condensate velocity $\vec{v}$ to vary smoothly in space, one obtains an equation of motion involving a metric tensor,

$$\frac{d^2x^\mu}{ds^2} = -\Gamma^\mu_{\alpha\beta}\frac{dx^\alpha}{ds}\frac{dx^\beta}{ds} + \frac{q}{m_V}F^{\mu\beta}\frac{dx^\alpha}{ds}g_{\alpha\beta}, \quad (10)$$

where $\Gamma^\mu_{\alpha\beta} = 0.5g^{\mu\nu}(\partial g_{\nu\alpha}/\partial x^\beta + \partial g_{\nu\beta}/\partial x^\alpha - \partial g_{\alpha\beta}/\partial x^\nu)$ are the Christoffel symbols, which appear because the metric, while remaining locally flat and of Minkowski type [with a Galilean transform of (9)], is allowed to vary. Here, g is the same metric tensor (3) as the one obtained for the weak density waves in a fluid [3] (the so-called "acoustic metric"). Physically, Eq. (3) means that the speed of the sound waves c arises as a maximal velocity limit for a vortex (as in special relativity), and all the terms containing v appear due to the Galilean transformations if the condensate is propagating in the laboratory frame.

If the vortex interaction forces and the Magnus force can be neglected, the test vortex is in the "free-fall" situation ($F_{\mu\nu} = 0$), described by the geodesic equation:

$$\frac{d^2x^\mu}{ds^2} = -\Gamma^\mu_{\alpha\beta}\frac{dx^\alpha}{ds}\frac{dx^\beta}{ds}. \quad (11)$$

The conditions required to neglect the forces acting on the vortex are discussed below in Sec. III C (see also Appendix C). The configurations with a non-negligible effective electromagnetic field tensor F could enable the study of electrodynamics in strongly curved spacetimes in future works.

B. Kerr black hole

The Kerr metric of a rotating black hole (in the equatorial plane only, since a 2D condensate can reproduce only a single plane) can be written in Boyer-Lindquist coordinates as

$$g^{\text{Kerr}}_{\mu\nu} = \begin{pmatrix} -\left(1 - \frac{2M}{r}\right) & 0 & -\frac{4aM}{r} \\ 0 & \frac{r^2}{r^2 - 2Mr + a^2} & 0 \\ -\frac{4aM}{r} & 0 & \left(r^2 + a^2 + \frac{2a^2M}{r}\right) \end{pmatrix}, \quad (12)$$

where a is the black hole angular momentum.

To reproduce such a metric, we consider a cylindrically symmetric configuration with radial and azimuthal flows (v_r, v_ϕ), with an appropriate change of coordinates [51], which allows us to write the metric of the condensate as

$$g_{\mu\nu} = \frac{mn}{c}\begin{pmatrix} -(c^2 - v^2) & 0 & -2rv_\phi \\ 0 & \left(1 - \frac{v_r^2}{c^2}\right)^{-1} & 0 \\ -2rv_\phi & 0 & r^2 \end{pmatrix}. \quad (13)$$

Here, the flow velocity $\mathbf{v}(\mathbf{r})$ and the speed of sound $c(\mathbf{r})$ are both functions of coordinates, determined by the unperturbed condensate wave function ψ. To obtain an analogue of a Kerr black hole, we need to generate a configuration where these functions would have a proper behavior. Quantum fluids are irrotational, and their azimuthal flow is controlled by the number ν of quantum vortices that are topological defects, characterized by the quantized circulation of angular velocity. On the other hand, a radial flow requires a sink (drain, particle decay) in the central region. Both can be combined using existing techniques [42] in polariton condensates: a macroscopically occupied state can be created or seeded by a Gauss-Laguerre beam carrying required angular momentum [52] (in the presence of a cw nonresonant or quasiresonant pumping), and a shorter lifetime can be provided by a localized defect in the cavity mirrors (or a μm-sized metal deposit) on which the beam should be centered.

Since even for a single vortex a complete analytical solution of the Gross-Pitaevskii equation has not been found yet, we use an asymptotic series expansion at $r \gg \xi$ in order to find ψ, where ξ is the size of a vortex core (the healing length). In this approximation, both the sink and the vorticity concentrated in the central region ($r \ll \xi$) can be approximated as δ functions:

$$\nabla \times \mathbf{v} = 2\pi\nu\frac{\hbar}{m}\delta_{2D}(\mathbf{r}), \qquad \nabla \cdot \mathbf{v} = -2\pi\zeta\frac{\hbar}{m}\delta_{2D}(\mathbf{r}), \quad (14)$$

where ν is an integer determining vorticity and $\zeta > 0$ is obtained *a posteriori* from particle decay in the center. This allows us to find the components of the velocity: $v_\phi = \hbar\nu/mr$, $v_r = \hbar\zeta/mr$, and the approximate solution for the wave function of the condensate:

$$\psi(r,\phi) = \sqrt{n_\infty}\left(1 - \xi^2\frac{\nu^2 + \zeta^2}{r^2}\right)\exp\left[i\left(\zeta\ln\frac{r}{\xi} + \nu\phi\right)\right]. \quad (15)$$

The scale of density variation is increased by $\sqrt{\nu^2 + \xi^2}$, ensuring a relatively slow metric variation for test waves and particles. Then, we find the analytical expressions for the radius of the event horizon r_h and the radius of the ergosphere (the static limit) r_s. Indeed, the event horizon is determined [53] by the change of sign of the metric component g_{rr} ($v_r = c$), which gives

$$r_H = \frac{\xi}{\sqrt{2}}(\zeta + \sqrt{3\zeta^2 + 2\nu^2}), \quad (16)$$

while the static limit is determined by the change of sign of g_{tt} ($v = c$), which gives

$$r_E = \frac{1 + \sqrt{3}}{\sqrt{2}}\xi\sqrt{\zeta^2 + \nu^2}. \quad (17)$$

As with the condensate wave function (15), both expressions are only valid if $r_{H,E} \gg \xi$.

First, we check that the proposed configuration is realistic and that the analytical solution is correct. To find the stationary solution for the condensate wave function containing $\nu = 16$ vortices in the short-lifetime region, we solve the Gross-Pitaevskii equation numerically with a relaxation term, using the typical parameters for GaAs cavities ($\alpha = 5\ \mu\text{eV}\,\mu\text{m}^2$, $m = 5 \times 10^{-5}m_0$ [54]; see Appendix A for details). The results are shown in Fig. 1. As expected, the initial single-vortex state with high angular momentum splits [39] into ν single-charged vortices kept inside the horizon by the convergent flow. Panel (a) shows the density profiles: the

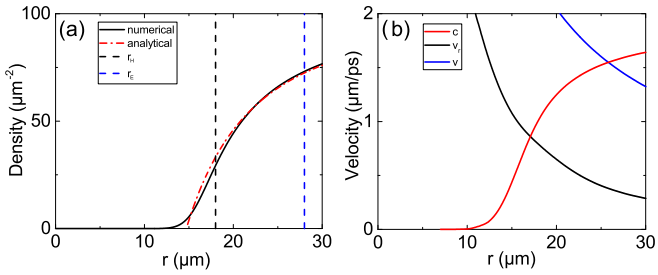

FIG. 1. Kerr black hole in a condensate. (a) Numerical solution of the Gross-Pitaevskii equation (black solid line) and the analytical density profile (red dash-dotted line). Black dashed line, horizon; blue dashed line, static limit. (b) Velocities determining the metric (from the numerical solution): c (black solid), v_r (blue dashed), and v (red dash-dotted).

analytical approximation with $\zeta \approx 7$ (red dash-dotted) gives a good fit to numerics (black solid) for $r > 16\ \mu$m, and the calculated positions of the event horizon (black dashed) and the static limit (blue dashed) are within the region of validity of the approximation. Their correctness is confirmed by the numerical velocities [panel (b)], their position given by the crossing of the speed of sound c (red) with the radial velocity v_r for the horizon (black) and total velocity v for the static limit (blue), with the ergoregion contained between the two.

C. Maximal angular momentum of the analogue Kerr black hole

As in general relativity, we find that the maximal angular momentum of the black hole analogue is limited by its mass. In general relativity, the maximal allowed value is $a_{\max}/M = 1$. One can rewrite this condition using the irreducible black hole mass (that of a nonrotating black hole), which we mark M_0: $a_{\max} = \sqrt{2}M_0$. To find the effective mass of the analogue black hole in a condensate, we begin by comparing the dominant term of the metric for a nonrotating BH in general relativity and in a condensate. In general relativity,

$$g_{rr} = \frac{2M_0}{r - r_H}, \tag{18}$$

while in the condensate

$$g_{rr} = \left(1 - \frac{v_r^2}{c^2}\right)^{-1} = \frac{1}{2}\frac{r_H}{r - r_H}, \tag{19}$$

which gives

$$M_0 = \frac{1}{4}r_H = \frac{1+\sqrt{3}}{4\sqrt{2}}\xi\zeta \approx 0.5\xi\zeta. \tag{20}$$

Therefore, the radius of the horizon is a good estimate for the analogue black hole mass:

$$M \sim r_H. \tag{21}$$

The maximal number of vortices $\nu_{\max}$ and thus the maximal angular momentum of a Kerr black hole analogue can be estimated as follows. When ν is increased, the centrifugal force expels vortices toward the horizon. This behavior is different from that of trapped rotating condensates, where vortices are usually forming a lattice [55]. Here, it is rather a chain of vortices that is formed [42] because of the effective

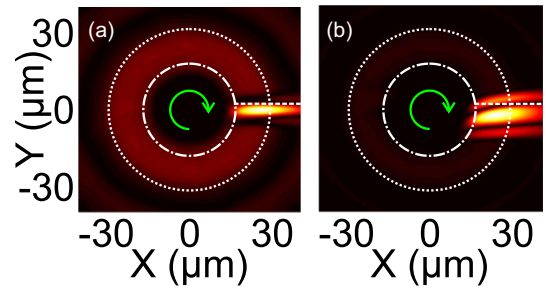

FIG. 2. Simulation of an acoustic Kerr black hole with a density wave. Images show the difference between the stationary solution ψ_0 and the perturbed solution $\psi(\mathbf{r}, t)$: (a) $t = 0$ (white dashed line marks the reference node of the density wave), (b) $t = 2$ ps (the node of the wave moves down inside the ergosphere and up outside). The dashed circle shows the static limit, and the dash-dotted circle shows the horizon. Green arrows mark the rotation direction.

energy profile. If $\nu_{\max}$ vortices are located along the horizon, the localization length for each of them can be estimated as

$$\xi' = \frac{2\pi r_H}{\nu_{\max}}. \tag{22}$$

The energy barrier that prevents vortices from escaping the black hole is given by the interaction energy $\mu = \alpha n$. This sets the condition for ξ':

$$\frac{\hbar^2}{2m}\left(\frac{2\pi}{\xi'}\right)^2 = \alpha n, \tag{23}$$

which allows us to express ξ' using the healing length ξ: $\xi' = 2\pi\xi$. We can then find $\nu_{\max}$:

$$\nu_{\max} = \frac{r_H}{\xi}. \tag{24}$$

Expressing the angular momentum a in the same natural units as the black hole mass M: $a_{\max} = \nu_{\max}\xi = r_H$, we obtain the maximal angular momentum of the analogue Kerr black hole:

$$\frac{a_{\max}}{M} \sim 1. \tag{25}$$

This is confirmed by the numerics. For the same parameters of localized decay as in Fig. 1, the numerical result for the maximal possible number of vortices is $\nu = 16$, which is indeed very close to the estimate $\nu_{\max} = r_H/\xi = 18$.

III. SIMULATIONS OF THE QUANTUM KERR BLACK HOLE ANALOG

A. Frame dragging

Next, we show that the behavior of the weak excitations of the condensate indeed corresponds to the metric (13). We solve the Gross-Pitaevskii equation (1) numerically over time, taking the condensate wave function ψ_0 found previously as an initial condition, maintaining constant particle density at a large distance. Weak density waves are created by a shallow, localized, and short potential pulse with a Gaussian shape. In practice, such a potential can be created by a laser pulse. Figure 2 shows two snapshots of the spatial images of the absolute value of the deviation from the stationary configuration $||\psi|^2 - |\psi_0|^2|$. Panel (a) shows a perturbation stretched along

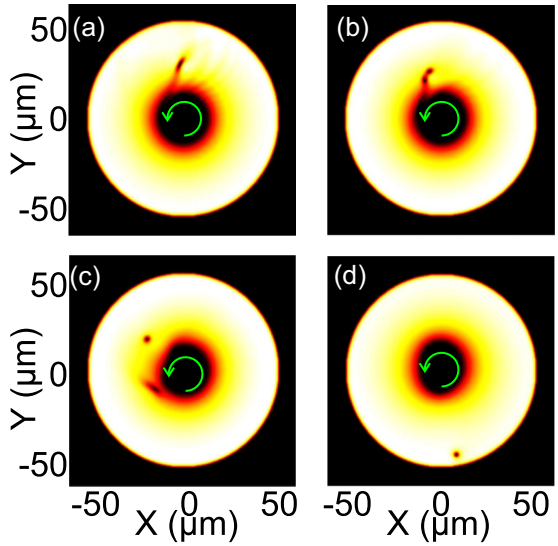

FIG. 3. Snapshots of the condensate density during the Penrose process. (a) Creation of a density dip; (b) formation of a vortex-antivortex pair; (c) annihilation of one of the vortices of the black hole; and (d) escape of the vortex. Green arrows mark the rotation direction.

the x axis, giving rise to two waves with radial velocities $\pm c$ with respect to the fluid. A node in this density wave used as a reference is marked by a dashed white line. Panel (b) shows the evolution of this image after 2 ps. As expected, inside the ergosphere (marked by a white dashed circle) both density waves propagate downward (in the direction of rotation of the black hole) due to frame dragging, whereas outside both propagation directions are possible.

B. Penrose process

Now that we have confirmed that our configuration provides a good analogy with a Kerr black hole for density waves (corresponding to null geodesics), we make the ultimate step, simulating a quantum analogue of the Penrose process with particles (vortices). In the Penrose process, a particle p entering the ergosphere separates into two particles p' and p'', with $E_{p''} < 0$, which allows the particle p' to have an energy higher than the initial one: $E_{p'} > E_p$ in spite of the energy conservation $E_p = E_{p'} + E_{p''}$.

The snapshots of the process for the analogue Kerr black hole are shown in Fig. 3 (see [56] for movies). We first discuss the process itself, and then analyze its microscopic details. We now use a strong localized potential pulse to create a strong density perturbation [Fig. 3(a)]. In a homogeneous condensate, this localized density dip corresponds to the final stage of a vortex-antivortex pair annihilation [39], propagating with a speed of sound c and disappearing with time. However, if such a density dip is created inside the ergosphere, the opposite effect is observed: the density dip becomes elongated because of the spaghettification [57], and a vortex-antivortex pair appears [Fig. 3(b)]. The antivortex, being closer to the horizon and corresponding to a negative-energy state $E < 0$, is rapidly absorbed by the black hole and annihilates a single vortex inside it [Fig. 3(c)], reducing its angular momentum.

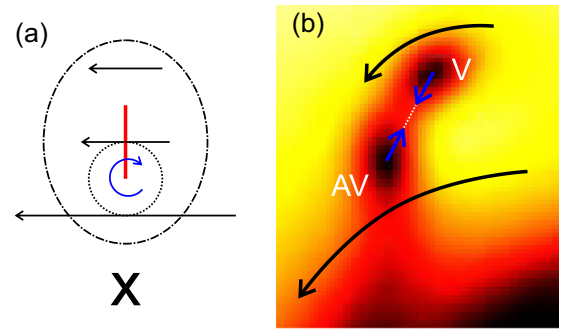

FIG. 4. (a) Scheme of the vortex formation from a density minimum due to a velocity gradient. (b) Vortex interaction bringing AV into a negative energy state and increasing the positive energy of V.

We stress the quantum nature of the analogue of the Penrose effect: in a quantum fluid, all rotation is concentrated in vortices, and can therefore change only in discrete steps. The remaining vortex, depending on the position of its creation, can either escape from the black hole to infinity [the edge of the cavity, Fig. 3(d)] or fall into the black hole.

To understand the quantum analogue of the Penrose process, we need to understand the formation of a pair of vortices. The density minimum created by a potential pulse could just disappear if the condensate were stationary. It is the gradient of the velocity of the flow close to the black hole that leads to the separation of this minimum into a vortex-antivortex pair. Indeed, the density minimum created in the condensate is deep enough to contain a zero-density line with undetermined phase. This line can spawn a pair of vortices if the conditions are favorable, which is indeed the case thanks to the velocity gradient [Fig. 4(a)]. We consider first the extreme point of the zero-density line (red line in the figure), closest to the center of the black hole (marked by a cross). The velocity circulation around this point (along the dashed circle) would have a tendency to become nonzero, if possible, and this can be realized by the formation of a vortex rotating in the direction opposite to that of the black hole (which we call an antivortex). Since the circulation around the dash-dotted line must remain zero (as it was initially), a vortex appears at the other end of the line, where the velocity gradient is much lower. In the end, it is this velocity gradient that breaks the symmetry and makes an antivortex appear closer to the black hole than the vortex.

Once the vortices are formed, it is the vortex-vortex "electromagnetic" interaction that brings the antivortex into the negative energy state [Fig. 4(b)]. Indeed, the vortices with opposite rotation are exhibiting a mutual attraction, as shown by the blue arrows along the white dashed line connecting their centers. In a stationary condensate, such attraction leads to the mutual annihilation of the vortex and the antivortex in the pair, but here it is not sufficient to overcome completely the attraction of the black hole. This interaction, as can be seen from the scheme, slows down the antivortex (AV) with respect to the flow while at the same time accelerating the vortex (V). This is the essential element of the analogue Penrose process in our system. Indeed, close to the horizon, *any* state rotating slower than the local zero-angular-momentum observer has

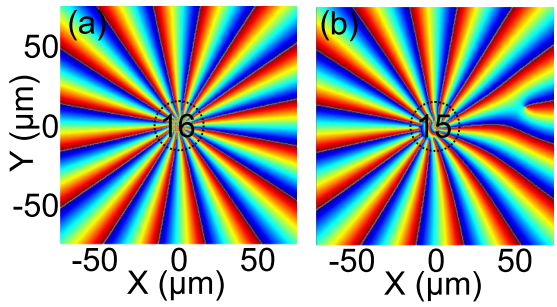

FIG. 5. Phase patterns for (a) stationary analogue Kerr black hole solution with $\nu = 16$; (b) $\nu = 15$ Kerr black hole after the Penrose process. The 16th vortex is visible on the right.

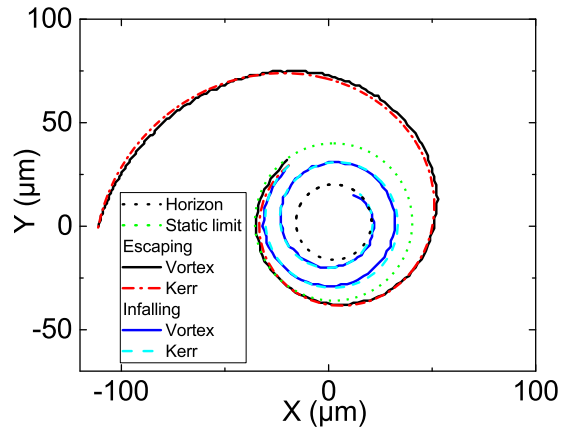

FIG. 6. Timelike geodesics. Trajectories of a quantum vortex (solid lines) and a massive particle (dashed/dash-dotted lines), in the vicinity of a Kerr black hole, exhibiting escaping (black, red) and infalling (blue, cyan) behavior. Dotted lines: horizon (black), static limit (green).

a negative energy [58] (which simply means that an energy higher than mc^2 is necessary to get the object to infinity). Therefore, the antivortex, being slowed down, gets into the state $E_{\rm AV} < 0$, and the vortex, being sped up, increases its energy (conserving the total). We have checked the velocity of the vortices from our numerical simulations and found that at the antivortex position the azimuthal velocity of the flow is $v_\phi = 1.6\ \mu$m/ps, whereas the antivortex velocity is $v_{\rm AV} = 1.4\ \mu$m/ps $< v_\phi$. So, the velocity of the antivortex is smaller than that of the flow, meaning that it is indeed in the negative energy state. We stress that this "electromagnetic" interaction is not, and is not supposed to be, described by the metric, exactly like the mechanism that separates the particle p into p' and p'' in the original Penrose process. It strongly depends on the V-AV distance and only plays a role at the first moments, whereas after the separation the free propagation of the vortex becomes well described by the metric.

The negative energy of the antivortex is confirmed by its velocity [58] and by the energy conservation (it allows the vortex to gain enough energy to escape). Indeed, a single vortex created at the same distance at $t = 0$ without the extra kinetic energy (that is, in a zero angular momentum state) always falls into the black hole. To confirm that the angular momentum of the black hole analogue is indeed decreasing, we show the phase of the condensate wave function before and after the Penrose process takes place. In Fig. 5 we see that the number of vortices in the black hole is reduced from $\nu = 16$ [panel (a)] to $\nu = 15$ [panel (b)] as a result of the Penrose process. We note that the ringdown effect of the perturbed black hole is also visible [59].

C. Timelike geodesics in analogue and general relativity metrics

Interestingly, the trajectory of the remaining vortex can be well described by the timelike geodesics of the Kerr metric. We use the Hamiltonian formulation of the Kerr geodesic motion, providing a better numerical stability [60], where the equations of motion, relevant for the equatorial plane, read

$$\dot{r} = \frac{\Delta}{\Sigma} p_r, \tag{26}$$

$$\dot{p_r} = -\left(\frac{\Delta}{2\Sigma}\right)' p_r^2 + \left(\frac{R}{2\Delta\Sigma}\right)', \tag{27}$$

$$\dot{\phi} = -\frac{1}{2\Delta\Sigma}\frac{\partial}{\partial L} R, \tag{28}$$

where a prime denotes a partial derivative over r, with $\Sigma = r^2$, $\Delta = r^2 - 2Mr + a^2$, $R = P^2 - \Delta[r^2 + (L - aE)^2]$, and $P = E(r^2 + a^2) - aL$. The integrals of motion for the test particle are its energy E and angular momentum L (fitting parameter). The comparison of the numerical simulations of the vortex propagation with the Gross-Pitaevskii equation (1) (solid lines) with the timelike geodesic trajectories (26) (dashed/dash-dotted lines) is shown in Fig. 6 (the system size is larger than in Fig. 3). A good agreement is obtained for both escaping and infalling trajectories, differing by their initial positions r.

We start the calculation of the geodesic trajectories of the Kerr metric by estimating the parameters of the black hole. To increase the size of the ergosphere and facilitate the observation of the Penrose process, we usually put the maximal possible number of vortices into the black hole, which corresponds to $a/M = 1$ in general relativity (see above). The value of M is chosen to correspond to the position of the horizon and of the static limit, known from the analytical wave function and numerical simulations. The fitting parameters are the angular momentum of the particle L and its initial radial momentum $p_r|_{t=0}$. The energy of the particle can be considered as fixed, because for any physically allowed values of the initial momentum determined by L and $p_r|_{t=0}$, one can choose a particle rest mass m_0 to keep the energy constant. The values of the fitting parameters change in agreement with the observed behavior of the vortex, as a function of the initial position of the density minimum. When the vortex is created closer to the black hole, it feels a higher attraction and higher azimuthal dragging, and therefore acquires a higher radial momentum $p_r|_{t=0}$ and higher angular momentum L during the Penrose process. The values used to fit Fig. 6 are $p_r = -0.01$, $L = 3.19$ for the escaping trajectory and $p_r = -0.4$, $L = 4.0$ for the infalling trajectory. The angular momentum of the black hole a changes during the Penrose process, but we consider the vortex trajectory only for its free propagation part, after the end of the Penrose process, when the antivortex has already been annihilated. During this free propagation part, the angular momentum of the black hole

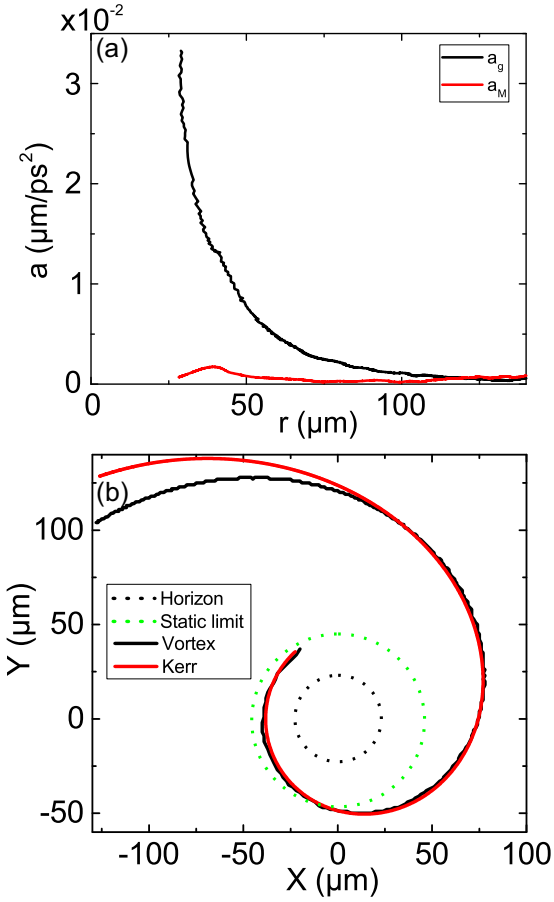

FIG. 7. (a) Comparison of the acceleration along the geodesic trajectory (black) with the acceleration due to the Magnus force (red). (b) Comparison of the vortex trajectory and the Kerr timelike geodesic at large distances.

does not change, and considering it as constant is a good approximation. Moreover, since $\nu \gg 1$, $\nu - 1 \approx \nu$, and it is still reasonable to take $a/M = 1$ even after the annihilation of one of the vortices of the black hole.

The agreement of analogue and real geodesic trajectories in the vicinity of the black hole requires two conditions to be fulfilled. First, the test vortex has to be in a "free-fall" situation, when "nongravitational" forces acting on it can be neglected. Second, the differences between the two metrics have to be negligible as well.

The nongravitational forces that can be included in the effective electromagnetic field tensor F in Eq. (10) are the interaction of vortices and the Magnus force. The part of the vortex-vortex interaction that is not captured by the metric is negligible for the test vortex for distances larger than ξ, which requires a sufficiently large horizon: $\sqrt{\nu^2 + \zeta^2} \gg 1$. The acceleration due to the Magnus force acting on the test vortex can be neglected with respect to the "free-fall" acceleration along a geodesic trajectory if the whole system is sufficiently large: $R \gg r_H$, because the momentum flux across the system boundary, responsible for this force, tends to zero (see Appendix C). Figure 7(a) shows the total acceleration along the vortex trajectory extracted from numerical simulations (black line) together with the acceleration due to the Magnus force (red line), for the calculation of which v' was obtained from the difference of the vortex velocity and the local velocity of the flow (both extracted from numerical simulations). This comparison confirms that the effect of the Magnus force is negligible for the part of the trajectory close to the horizon. The noise on both curves is due to the fact that the vortex position can only be determined up to the grid step, and the acceleration is its second derivative, which amplifies the quantization noise.

The differences between the original Kerr metric Eq. (12) in general relativity and the condensate Kerr metric Eq. (13) become negligible close to the horizon thanks to the fact that the motion is mostly determined by the divergent metric term g_{rr}, behaving as $g_{rr} \sim (r - r_H)^{-1}$ for both of them. We stress that at large distances, the condensate metric gives an effective potential $U_{\rm cond} \sim -1/r^2$ *different* from that of the Kerr metric $U_{\rm Kerr} \sim -1/r$, leading to the deviation of the trajectory from the predictions of general relativity. Moreover, the vortex interaction with the wall becomes dominant at $R - r \approx \xi$. To illustrate the differences between the true and the analogue Kerr metrics, we made a larger-scale calculation, which shows that while the Kerr geodesic fits the vortex trajectory very well at short distances, the two diverge at larger r. A faster decay of the effective gravitational potential in the condensate means that the characteristic distances are reduced: for the same kinetic energy, the vortex goes less far away than a particle in the true Kerr metric. This is what is observed in Fig. 7(b): the Kerr geodesic (red line) fits the vortex trajectory (black line) very well at short distances, while at larger scales the vortex starts to lose the kinetic energy faster.

That said, the most important fact is that the condensate metric correctly reproduces the behavior in the immediate vicinity of the horizon, confirming that an analogue metric can be sufficiently close to the Kerr metric at least in the most important region for the simulation of Kerr black holes.

IV. DISCUSSION AND CONCLUSIONS

Although we dealt with a quantum fluid, similar phenomena could also be observable to some extent in classical fluids [31,32]. We stress that our simulations in the mean-field approximation neglect the quantum fluctuations. However, these fluctuations represent one of the most interesting features of the analogue systems, which make the scales of quantum mechanics and general relativity comparable. The natural outlook of the present work is therefore the study of the effect of quantum fluctuations (controlled via the condensate density, see Appendix B) and the elucidation of quantum effects in analogue gravity experiments by comparison with mean-field predictions for the development of quantum gravity [6]. Another important direction could be the study of effective electrodynamics in strongly curved spacetimes, with vortices and bogolons playing the role of charges and photons. Finally, our work marks an important step toward self-consistent analogue gravity: the metric in our case is not completely fixed externally, but depends on the matter and energy (vortex) distribution in the system.

To conclude, we have shown that a Kerr black hole with quantized angular momentum can be created in a condensate in the presence of a localized particle decay, and that the

quantum vortices as test particles close to such an analogue black hole follow the timelike geodesics given by the general relativity for the Kerr metric. This configuration, therefore, represents a unique possibility to observe experimentally the propagation of massive particles along strongly non-Newtonian geodesics, far beyond the small relativistic corrections of the Mercury orbit. Finally, we have demonstrated a quantum analogue of the Penrose effect, extracting the rotation energy of a Kerr black hole in discrete steps.

ACKNOWLEDGMENTS

We acknowledge useful discussions with S. Weinfurtner and T. Torres. We acknowledge the support of the project "Quantum Fluids of Light" (ANR-16-CE30-0021), of the ANR Labex Ganex (ANR-11-LABX-0014), and of the ANR program "Investissements d'Avenir" through the IDEX-ISITE initiative 16-IDEX-0001 (CAP 20-25). D.D.S. acknowledges the support of IUF (Institut Universitaire de France). S.V.K. acknowledges the support from the Ministry of Education and Science of the Russian Federation (SPbAU RAS Project No. 16.9790.2017/BCh).

APPENDIX A: NUMERICAL SIMULATIONS

We have performed the simulations using mesh sizes between $N \times N = 2^8 \times 2^8$ and $N \times N = 2^{10} \times 2^{10}$, with $h = 0.5$ μm step size. The time step was $dt = 2 \times 10^{-15}$ s. We used the third-order Adams-Bashforth method for the time integration of the Gross-Pitaevskii equation, both with and without the relaxation term (see below). The Laplacian term was calculated via a double Fourier transform in order to obtain an efficient parallelization on the graphics processing unit.

The polariton density and the interaction constant were chosen to have the interaction energy $\mu = \alpha n_\infty = 1$ meV. The potential U has both real and imaginary parts: $U = U_c(\mathbf{r}) - i\Gamma(\mathbf{r})$, where the real part describes an etched cylindrical mesa of a large diameter $R = 100$ μm (or larger for some calculations) providing the confinement of the condensate: $U_c(\mathbf{r}) = U_0\Theta(r - R)$, where Θ is the Heaviside function. The imaginary part ensures the convergent polariton flow toward the center. It describes a localized defect increasing the particle annihilation rate (e.g., defect in the cavity mirrors or a micrometric size metallic droplet on their surface): $\Gamma(\mathbf{r}) = \frac{\hbar}{2\tau} e^{-\frac{r^2}{2\sigma^2}}$, where $\sigma = 6$ μm is the size of the defect. The effective decay rate for the analytical approximation ζ discussed in the main text can be approximated as the average value $\langle\psi|\Gamma(r)|\psi\rangle$. It plays a role of a fitting parameter for Figs. 1(a) and 1(b) of the main text. We stress that contrary to the vorticity ν, the decay parameter ζ is not quantized and does not have to be an integer.

To find the stationary solution of the Gross-Pitaevskii equation numerically, we introduce the phenomenological damping term proposed by Pitaevskii in 1958 to describe the energy relaxation [61]. The damped Gross-Pitaevskii equation reads

$$i\hbar\frac{\partial\psi}{\partial t} = (1 - i\Lambda)\left(-\frac{\hbar^2}{2m}\Delta\psi + \alpha|\psi|^2\psi + U\psi - \mu\psi\right), \tag{A1}$$

where Λ is a dimensionless damping coefficient, which for reasonable calculation time and precision can range from 10^{-3} to 10^{-1}.

A stationary solution ψ_0 of the nondamped Gross-Pitaevskii equation with an energy μ is also a solution of the damped equation: the right part of the equation simply vanishes and the presence of Λ does not change anything. Moreover, any perturbations to the stationary solution ψ_0 increasing its energy tend to decay, and their decay rate is proportional to their energy deviation from μ. This procedure conserves zeros of the wave function, and therefore allows us to find stationary solutions different from the ground state, starting from an appropriate initial wave function. To improve convergence, we start with the initial wave function

$$\psi(r, \phi) = \sqrt{n_\infty}\tanh\frac{r}{\xi}\Theta(R - r)\exp i\nu\phi. \tag{A2}$$

The initial state with a single high-winding vortex is split into ν single-winding vortices, which remain inside the horizon. The wave function ψ_0 found by the above numerical procedure is then used as a stationary solution on which the perturbations are created by time-dependent potential pulses.

To implement a stationary convergent flow, we maintain a constant particle density far from the central region. This is equivalent to the experimentally realistic situation of nonresonant pumping with a ringlike profile, which maintains the condensate at a constant level. To perturb the condensate, we use an extra term in the real part of the potential profile $\delta U(\mathbf{r}, t)$ with a different shape:

(i) For Fig. 2, we used a Gaussian-shaped potential pulse strongly elongated along the x axis. The pulse is also Gaussian in time:

$$\delta U(\mathbf{r}, t) = \delta U_0 e^{-\frac{(x-x_0)^2}{2\sigma_x^2}} e^{-\frac{(y-y_0)^2}{2\sigma_y^2}} e^{-\frac{(t-t_0)^2}{2\sigma_t^2}}, \tag{A3}$$

where $\sigma_x = 30$ μm, $\sigma_y = 3$ μm, and $\sigma_t = 0.5$ ps. The size of the perturbation along the y axis has to be large enough ($\sigma_y \gg \xi$) in order not to involve large wave-vector bogolons, which propagate faster than the speed of sound c. At the same time, it has to remain small enough in order to remain along a single azimuthal direction. The amplitude here was $\delta U_0 = 0.1$ meV, much smaller than the interaction energy αn_∞.

(ii) For Fig. 3, the size of the pulse has to be comparable with the size of a vortex pair 2ξ:

$$\delta U(\mathbf{r}, t) = \delta U_0 e^{-\frac{(x-x_0)^2}{2\sigma_x^2}} e^{-\frac{(y-y_0)^2}{2\sigma_y^2}} e^{-\frac{(t-t_0)^2}{2\sigma_t^2}} \tag{A4}$$

with $\sigma_x = 3$ μm, $\sigma_y = 1$ μm, and $\sigma_t = 0.5$ ps. The orientation of this slightly elongated density minimum influences the splitting and the trajectories of the vortex and antivortex. We have kept this orientation along the y axis in order to have a limited number of variable parameters in the system.

APPENDIX B: MEAN-FIELD THEORY AND FLUCTUATIONS

In the present work, we neglect the quantum and thermal fluctuations of the condensate, limiting the consideration to the mean-field approach. In 2D systems at 0 K, quantum fluctuations lead to a depletion of the condensate determined by the interactions [39]. In 2D, the quantum depletion can be

estimated from the one-body density matrix, as the relative difference between its value at zero distance (local correlations determined by both the condensed and the excited fractions) and at infinity (determined only by the condensate, by the definition of the long-range order):

$$\frac{n^{(1)}(0)-n^{(1)}(\infty)}{n^{(1)}(0)} \sim \frac{1}{n\xi^2} \sim \frac{\alpha m}{\hbar^2}. \tag{B1}$$

We see that the relative importance of quantum depletion can be controlled via the interactions or the particle mass, which can be tuned by using the Feshbach resonance (in atomic condensates) and the detuning (in polariton condensates). On the one hand, this should allow to reproduce the mean-field results obtained in the present paper by reducing the interactions and the mass. On the other hand, increasing the effect of the quantum fluctuations paves the way toward analogue quantum gravity. Comparing the results obtained in the two regimes could allow us to make clear the effects of a fluctuating metric.

At nonzero temperatures, thermal fluctuations induce a power-law decay of the coherence:

$$n^{(1)}(s) \sim \left(\frac{s_T}{s}\right)^{\nu} \tag{B2}$$

with

$$\nu = \frac{k_B T m}{2\pi\hbar^2 n_s}, \tag{B3}$$

where n_s is the superfluid density. For polaritons at 10 K (typical for GaAs cavities providing the best quality), $s_T \approx 1.3\ \mu$m and $\nu \approx 5\times10^{-4}$, which gives a very slow decay of the condensate coherence with respect to all other possible sources. We therefore expect that thermal fluctuations should not cause too many problems for the observation of the effects discussed in the main text.

APPENDIX C: MAGNUS FORCE EFFECT FOR THE TEST VORTEX

While the derivation of the Magnus force has become textbook material, its presence or absence in particular conditions is a highly controversial subject, especially in superconductors [62]. In uncharged quantum fluids, its presence is established better [63].

We begin with the derivation of the Magnus force in a general case [64]. A vortex in a fluid creates a velocity field

$$\mathbf{v} = \frac{\hbar}{m}\frac{1}{\eta}\mathbf{e}_\phi, \tag{C1}$$

where $\mathbf{e}_\phi$ is a unit vector in the azimuthal direction and η is the radial coordinate. At the same time, there is a background flow with velocity $\mathbf{v}'$. The momentum-flux tensor is given by

$$\Pi_{ij} = P\delta_{ij} + \rho(v_i - v_i')(v_j - v_j'), \tag{C2}$$

where the relevant terms for the pressure P appearing due to Bernoulli's law are

$$P\delta_{ij} = -\tfrac{1}{2}\rho(v_i - v_i')^2 - \tfrac{1}{2}\rho(v_j - v_j')^2. \tag{C3}$$

The force acting on the vortex line is equal to the total momentum flux through a boundary surrounding this vortex line:

$$F_i = \oint dS_j \Pi_{ij}. \tag{C4}$$

Let us consider a circular boundary with a radius r_0, assuming $\mathbf{v}' = v_x'\mathbf{e}_x$. The relevant terms of the elementary momentum flux at the two points located at $(r_0, 0)$ and $(-r_0, 0)$ are

$$dF_y = \Pi_{yx} dS_x = +\left(-\frac{1}{2}\rho v_y^2 - \frac{1}{2}\rho {v'}^2{}_x + \rho v_y v_x'\right) r_0 d\phi \tag{C5}$$

and

$$dF_y = \Pi_{yx} dS_x = -\left(-\frac{1}{2}\rho v_y^2 - \frac{1}{2}\rho {v'}^2{}_x - \rho v_y v_x'\right) r_0 d\phi, \tag{C6}$$

which give a net elementary momentum flux of

$$dF_y = \rho v_x' \frac{\hbar}{m}\frac{1}{r_0} r_0 d\phi, \tag{C7}$$

which does not depend on the radius of the integration contour r_0. These terms do not cancel because while the fluid velocity v_x' has the same sign at both boundaries, the vortex field velocity v_y changes sign, and the vector of the normal to the surface dS_x changes sign as well.

Integrating (C7), one obtains the expression for the Magnus force

$$F = 2\pi\hbar n v' \tag{C8}$$

similar to the Kutta-Joukowski theorem.

However, it is important to understand that while the vortex itself is a single zero-density point, its motion implies the modification of the whole velocity field. This is why the system size appears in the expression for the vortex mass, and in an infinite system this mass would be infinite. The conservation of momentum allows us to consider a contour of any radius in Eq. (C4), and the result does not depend on this choice. This is not true in a system with a sink that we consider. To find the total force acting on the vortex as a part of a global velocity field, we need to calculate the momentum flux over a surface surrounding the whole system. At this scale, one cannot assume the fluid flow to have a constant velocity $\mathbf{v}'$. The momentum flux is associated with the flow crossing the integration contour, that is, mostly with the convergent flow given by $v_r = -\hbar\zeta/mR$ (R is the system size), which gives the main contribution to the relative velocity of the vortex with respect to the fluid. The momentum flux in two opposite points will therefore be proportional to

$$dF_y \sim R\frac{\hbar\zeta}{m}\left(\frac{1}{R-r} - \frac{1}{R+r}\right) \sim \frac{r}{R}. \tag{C9}$$

The Magnus force is therefore reduced by a factor r/R, where r is the displacement of the vortex with respect to the center of the black hole. This occurs because the fluid flow is not homogeneous at the system's scale.

It allows us to neglect the Magnus force when the system size is sufficiently large with respect to the scale of the "free-fall" trajectories that are supposed to correspond to the geodesics of the Kerr metric. It means $R \gg r_H$, because the two metrics are similar only close to the horizon.

To check that the effects of the Magnus force are indeed small, we compare the acceleration due to the Magnus force with the total acceleration of the vortex with respect to a remote observer (given by the motion along the "free-fall" trajectory).

Taking into account the vortex mass, the acceleration due to the Magnus force is given by

$$a_M = \frac{2\alpha n v'}{\hbar \ln R/\xi}\frac{r}{R} \tag{C10}$$

while the acceleration along the geodesic trajectory can be estimated as

$$a_g = \frac{\hbar^2 v^2}{m^2 r^3}. \tag{C11}$$

With the parameters used in the simulations, the ratio of the two accelerations close to the horizon is about 2.5%.

The results of corresponding numerical simulations are shown in the main text (Fig. 7).

[1] S. W. Hawking, Nature (London) **248**, 30 (1974).
[2] T. Kibble, J. Phys. A **9**, 1387 (1976).
[3] W. G. Unruh, Phys. Rev. Lett. **46**, 1351 (1981).
[4] W. Zurek, Nature (London) **317**, 505 (1985).
[5] G. Volovik, *The Universe in a Helium Droplet* (Clarendon, Oxford, 2003).
[6] C. Barceló, S. Liberati, and M. Visser, Living Rev. Relativ. **8**, 12 (2005).
[7] C. Barcelo, Nat. Phys. **15**, 210 (2019).
[8] S. Weinfurtner, E. W. Tedford, M. C. J. Penrice, W. G. Unruh, and G. A. Lawrence, Phys. Rev. Lett. **106**, 021302 (2011).
[9] J. Steinhauer, Nat. Phys. **10**, 864 (2014).
[10] M. J. Bowick, L. Chandar, E. A. Schiff, and A. M. Srivastava, Science **263**, 943 (1994).
[11] L. Feng, L. W. Clark, A. Gaj, and C. Chin, Nat. Phys. **14**, 269 (2018).
[12] I. Bloch, J. Dalibard, and S. Nascimbene, Nat. Phys. **8**, 267 (2012).
[13] *Analogue Gravity Phenomenology*, edited by D. Faccio, F. Belgiorno, S. Cacciatori, V. Gorini, S. Liberati, and U. Moschella (Springer, Heidelberg, 2013).
[14] N. P. Armitage, E. J. Mele, and A. Vishwanath, Rev. Mod. Phys. **90**, 015001 (2018).
[15] S. Eckel, A. Kumar, T. Jacobson, I. B. Spielman, and G. K. Campbell, Phys. Rev. X **8**, 021021 (2018).
[16] A. Kavokin, J. J. Baumberg, G. Malpuech, and F. P. Laussy, *Microcavities* (Oxford University Press, Oxford, 2011).
[17] E. Wertz, L. Ferrier, D. Solnyshkov, R. Johne, D. Sanvitto, A. Lemaitre, I. Sagnes, R. Grousson, A. Kavokin, P. Senellart *et al.*, Nat. Phys. **6**, 860 (2010).
[18] D. Sanvitto, S. Pigeon, A. Amo, D. Ballarini, M. De Giorgi, I. Carusotto, R. Hivet, F. Pisanello, V. Sala, P. Guimaraes *et al.*, Nat. Photon. **5**, 610 (2011).
[19] D. D. Solnyshkov, H. Flayac, and G. Malpuech, Phys. Rev. B **84**, 233405 (2011).
[20] D. Gerace and I. Carusotto, Phys. Rev. B **86**, 144505 (2012).
[21] D. D. Solnyshkov, A. V. Nalitov, and G. Malpuech, Phys. Rev. Lett. **116**, 046402 (2016).
[22] R. Hivet, H. Flayac, D. D. Solnyshkov, D. Tanese, T. Boulier, D. Andreoli, E. Giacobino, J. Bloch, A. Bramati, G. Malpuech *et al.*, Nat. Phys. **8**, 724 (2012).
[23] H. S. Nguyen, D. Gerace, I. Carusotto, D. Sanvitto, E. Galopin, A. Lemaître, I. Sagnes, J. Bloch, and A. Amo, Phys. Rev. Lett. **114**, 036402 (2015).
[24] R. Penrose and R. M. Floyd, Nat. Phys. Sci. **229**, 177 (1971).
[25] R. P. Kerr, Phys. Rev. Lett. **11**, 237 (1963).
[26] R. Narayan, J. E. McClintock, and A. Tchekhovskoy, *Energy Extraction from Spinning Black Holes Via Relativistic Jets* (Springer International, Switzerland, 2014).
[27] K. Akiyama *et al.* (The Event Horizon Telescope Collaboration), Astrophys. J., Lett. **875**, L1 (2019).
[28] M. Visser, Class. Quantum Grav. **15**, 1767 (1998).
[29] D. Vocke, C. Maitland, A. Prain, K. E. Wilson, F. Biancalana, E. M. Wright, F. Marino, and D. Faccio, Optica **5**, 1099 (2018).
[30] O. Lahav, A. Itah, A. Blumkin, C. Gordon, S. Rinott, A. Zayats, and J. Steinhauer, Phys. Rev. Lett. **105**, 240401 (2010).
[31] L.-P. Euvé, F. Michel, R. Parentani, T. G. Philbin, and G. Rousseaux, Phys. Rev. Lett. **117**, 121301 (2016).
[32] T. Torres, S. Patrick, A. Coutant, M. Richartz, E. W. Tedford, and S. Weinfurtner, Nat. Phys. **13**, 833 (2017).
[33] S. Basak and P. Majumdar, Class. Quantum Grav. **20**, 3907 (2003).
[34] V. N. Popov, Zh. Eksp. Teor. Fiz. **64**, 672 (1973) [JETP **37**, 341 (1973)].
[35] J. C. Maxwell, Philos. Mag. **90**, 11 (1861).
[36] V. Ambegaokar, B. I. Halperin, D. R. Nelson, and E. D. Siggia, Phys. Rev. B **21**, 1806 (1980).
[37] V. N. Popov, *Continual Integrals in Quantum Field Theory and Statistical Physics* (Atomizdat, Moscow, 1976).
[38] P.-M. Zhang, L.-M. Cao, Y.-S. Duan, and C.-K. Zhong, Phys. Lett. A **326**, 375 (2004).
[39] L. Pitaevskii and S. Stringari, *Bose-Einstein Condensation*, International Series of Monographs on Physics 116 (Oxford Science Publications, Oxford, 2003).
[40] D. V. Freilich, D. M. Bianchi, A. M. Kaufman, T. K. Langin, and D. S. Hall, Science **329**, 1182 (2010).
[41] G. Nardin, G. Grosso, Y. Leger, B. Pietka, F. Morier-Genoud, and B. Deveaud-Pledran, Nat. Phys. **7**, 635 (2011).
[42] T. Boulier, H. Tercas, D. D. Solnyshkov, Q. Glorieux, E. Giacobino, G. Malpuech, and A. Bramati, Sci. Rep. **5**, 9230 (2015).
[43] H. Ohadi, R. L. Gregory, T. Freegarde, Y. G. Rubo, A. V. Kavokin, N. G. Berloff, and P. G. Lagoudakis, Phys. Rev. X **6**, 031032 (2016).
[44] H. Takeuchi, M. Tsubota, and G. E. Volovik, J. Low Temp. Phys. **150**, 624 (2008).
[45] C. Michel, O. Boughdad, M. Albert, P.-E. Larre, and M. Bellec, Nat. Commun. **9**, 2108 (2018).
[46] L. J. Garay, J. R. Anglin, J. I. Cirac, and P. Zoller, Phys. Rev. Lett. **85**, 4643 (2000).
[47] F. J. Dyson, Am. J. Phys. **58**, 209 (1990).
[48] P. A. M. Dirac, Nature (London) **168**, 906 (1951).
[49] V. N. Popov, Theor. Math. Phys. **6**, 65 (1971).

[50] V. N. Popov, Theor. Math. Phys. **11**, 478 (1972).
[51] E. Berti, V. Cardoso, and J. P. S. Lemos, Phys. Rev. D **70**, 124006 (2004).
[52] F. M. Marchetti, M. H. Szymańska, C. Tejedor, and D. M. Whittaker, Phys. Rev. Lett. **105**, 063902 (2010).
[53] M. Visser and S. Weinfurtner, Class. Quantum Grav. **22**, 2493 (2005).
[54] L. Ferrier, E. Wertz, R. Johne, D. D. Solnyshkov, P. Senellart, I. Sagnes, A. Lemaître, G. Malpuech, and J. Bloch, Phys. Rev. Lett. **106**, 126401 (2011).
[55] J. R. Abo-Shaeer, C. Raman, J. M. Vogels, and W. Ketterle, Science **292**, 476 (2001).
[56] See Supplemental Material at http://link.aps.org/supplemental/10.1103/PhysRevB.99.214511 for movies depicting the process for the analogue Kerr black hole.
[57] S. Hawking, *A Brief History of Time* (Bantam, New York, 1988).
[58] E. F. Taylor, J. A. Wheeler, and E. Bertschinger, *Exploring Black Holes: Introduction to General Relativity* (Addison-Wesley Longman, 2017).
[59] S. Patrick, A. Coutant, M. Richartz, and S. Weinfurtner, Phys. Rev. Lett. **121**, 061101 (2018).
[60] J. Levin and G. Perez-Giz, Phys. Rev. D **77**, 103005 (2008).
[61] L. P. Pitaevskii, J. Exptl. Theoret. Phys. (U.S.S.R.) **35**, 408 (1958) [JETP **8**, 282 (1959)].
[62] P. Ao and D. J. Thouless, Phys. Rev. Lett. **70**, 2158 (1993).
[63] W. F. Vinen, Nature (London) **181**, 1524 (1958).
[64] L. D. Landau and E. M. Lifshitz, *Fluid Hydrodynamics* (Pergamon, Oxford, 1987).